Supporting Information

Optical Activity and Optical Anisotropy in Photomechanical Crystals of Chiral Salicylidenephenylethylamines

Akifumi Takanabe,[†] Masahito Tanaka,[‡] Kohei Johmoto,[§] Hidehiro Uekusa,[§] Tadashi Mori,[‖] Hideko Koshima,[*,⊥] and Toru Asahi[*,†,⊥]

[†]Department of Advanced Science and Engineering, Graduate School of Advanced Science and Engineering, Waseda University, 3-4-1 Okubo, Shinjuku-ku, Tokyo 169-8555, Japan

[‡]Research Institute for Measurement and Analytical Instrumentation, National Institute of Advanced Industrial Science and Technology (AIST), Tsukuba Central 2, 1-1-1 Umezono, Tsukuba, Ibaraki 305-8568, Japan

[§]Department of Chemistry and Materials Science, Graduate School of Science and Engineering, Tokyo Institute of Technology, 2-12-1 Ookayama, Meguro-ku, Tokyo 152-8551, Japan

[‖]Department of Applied Chemistry, Graduate School of Engineering, Osaka University, 2-1 Yamada-oka, Suita, Osaka 565-0871, Japan

[⊥]Researh Organization for Nano & Life Innovation, Waseda University, 513 Wasedatsurumaki-cho, Shinjuku-ku, Tokyo 162-0041, Japan

Contents:

irradiation: CB (dark blue circle) and CD (dark blue triangle) (c) without and (d) with UV irradiation. The curve lines of LB and CB are served as an eye guide, and those of LD and CD are fitted by Gaussian functions. All the graphs indicate that the Kramers–Kronig relationship hold between (a, b) the LD and LB as well as (c, d) the CD and CB before and under continuous UV irradiation.

Figure S7. (a) Time dependence and (b) spot dependence of surface temperature change of the enol-(*S*)-**1** crystal upon UV (365 nm) irradiation measured by IR thermometer (Apiste FSV-2000). (c) IR thermographic image. The crystal form is lined in black color. The spot numbers are manually defined. (d) The right drawing represents the thin platelike crystal fixed on a Cu sample plate with a pinhole of 0.5 mm in diameter. The left drawing represents the enlarged view of the white rectangle box area. The white scale bar is 0.5 mm.

Figure S8. (a) In situ surface temperature profile of the enol-(*S*)-**1** crystal measured by IR thermometer (JAPAN SENSOR TMHX-CSE0500-0040H0.7) and (b) schematic representation of *in situ* surface temperature measurement. In the graph (a), the thin platelike crystal fixed on the Cu plate was mounted on the sample stage of the HAUP apparatus. The measurement area of the IR thermometer was 0.7 mm in diameter. Black line: none means no incident light of the HAUP (blank). Red line: HAUP means that the sample was irradiated by the incident light (330 nm) during the HAUP measurement. Blue line: UV means that the sample was irradiated with UV-LED light at 365 nm for proceeding the photoisomerization to the *trans*-keto-(*S*)-**1**. Pink line: HAUP + UV means that the sample was irradiated by both the incident light of HAUP (330 nm) and UV-LED light (365 nm). The each measurement time interval was 45 min.

Figure S9. Optical anisotropic and chiroptical spectra of enol-(*S*)-**1** and enol-(*R*)-**1** crystals on the (001) face: (a) LB, (b) LD, (c) CB, and (d) CD. These properties were measured with the G-HAUP without and under continuous UV light irradiation at 365 nm. The curve lines are served as an eye guide (a, c) and are fitted by Gaussian functions (b, d).

Figure S10. Visualization of (b, d) HOMO and (a, c) LUMO orbitals involved in the electronic transitions of calculated (a, b) enol-(*S*)-**1** and (c, d) *trans*-keto-(*S*)-**1**. All molecules are projected on the (001) face. Orbitals of HOMO and LUMO are of π type. See the Experimental Section in the main text for calculation details.

Figure S11. Bending behavior of a platelike enol-(*S*)-**1** crystal (4516 μm long × 380 μm wide × 97 μm thick) (a) before and upon irradiation from left to the (00–1) face with (b) linearly polarized UV light parallel and (c) perpendicular vibration direction to the *a* axis. The scale bar is 1 mm. To produce a linearly polarized light, Glan-Tompson prism polarizer was applied between the sample and the UV LED light illuminator. Because of the presence of the Glan-Tompson prism polarizer, the intensity of the UV light was decreased (30 mW cm^{-2}).

Figure S12. LD spectra of the enol-(*S*)-**1** crystal before (yellow open circle) and under continuous UV light irradiation (orange open circle) calculated from the linearly polarized absorption spectra in Figure 5 of the main text. The curve lines are fitted by Gaussian functions.

Figure S13. Optical anisotropic properties of (a, b) enol-(*S*)-**1** and (c, d) enol-(*R*)-**1** crystals on the (001) face: (a, c) LB and (b, d) LD without and with UV irradiation. The curve lines are served as an eye guide (a, c) and are fitted by Gaussian functions (b, d).

Figure S14. (a) Optical rotation, (b) CD, and (c) UV-Vis absorption spectra of enol-(*S*)-1 (blue) and enol-(*R*)-1 (pink) in hexane (c 0.016). Concentration in g $(100\ mL)^{-1}$.

Figure S15. (a) ORP and (b) CD spectra of enol-(*S*)-**1** and enol-(*R*)-**1** crystals on the (001) face before and under continuous UV irradiation. The curve lines are served as an eye guide (a) and are fitted by Gaussian functions (b).

Table S1. Cartesian Atomic Positions for enol-(*S*)-**1** generated from the calculated crystal structure.

Table S2. Cartesian Atomic Positions for *trans*-keto-(*S*)-**1** generated from the calculated crystal structure.

Movie S1. Bending with twisting motion of a wide and thin platelike microcrystal of enol-(*S*)-**1** (354 μm long × 87 μm wide × 10 μm thick) when the (00−1) face was irradiated by UV light.

Movie S2. Bending with twisting motion of a wide and thin platelike microcrystal of enol-(*S*)-**1** (354 μm long × 87 μm wide × 10 μm thick) when the (001) face was irradiated by UV light.

Movie S3. Bending behavior of a platelike enol-(*S*)-**1** crystal (4516 μm long × 380 μm wide × 97 μm thick) when the (00−1) face was irradiated by linearly polarized UV light whose vibration axis is parallel to the *a* axis.

Movie S4. Bending behavior of a platelike enol-(*S*)-**1** crystal (4516 μm long × 380 μm wide × 97 μm thick) when the (00−1) face was irradiated by linearly polarized UV light whose vibration axis is perpendicular to the *a* axis.

References

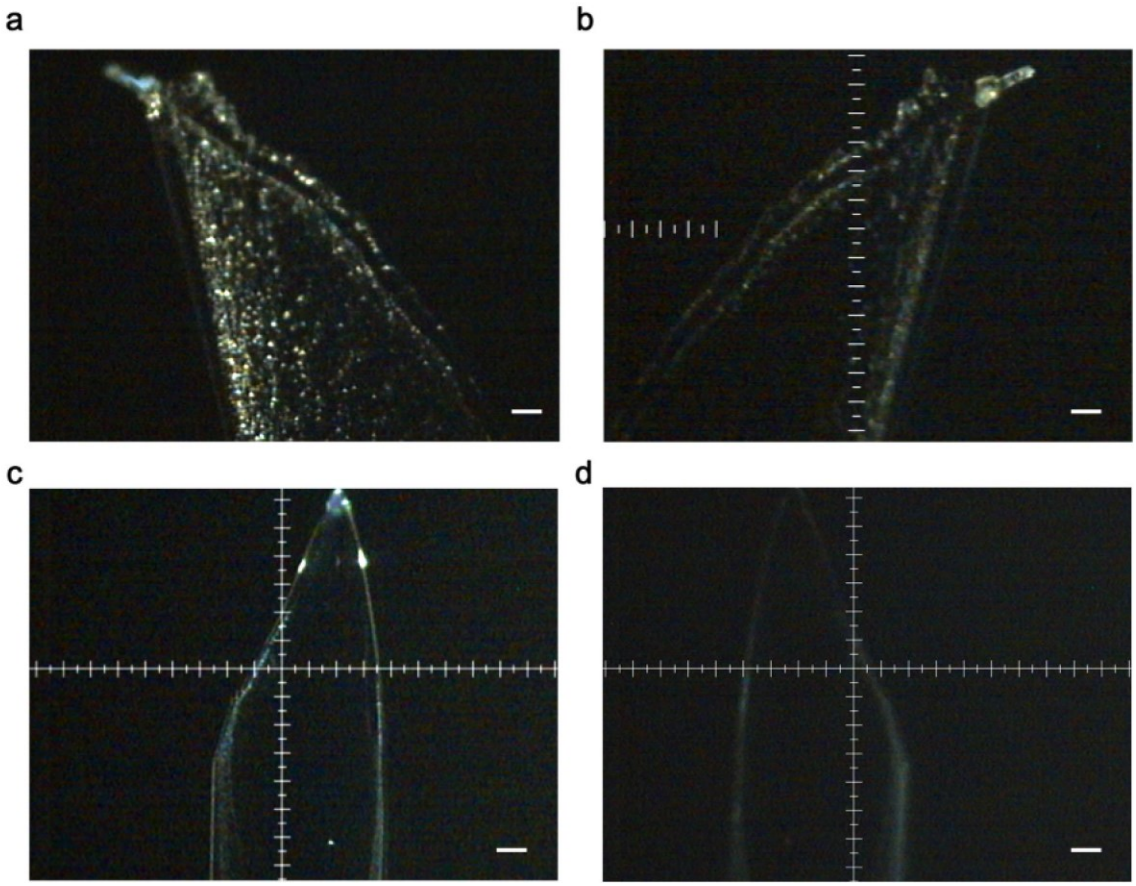

Figure S1. Crystal shapes of (a, b) enol-(*S*)-**1** and (c, d) enol-(*R*)-**1** crystal; the top surface (a, c) (00−1) face and (b, d) (001) face. All the faces were determined by using the single crystal X-ray structure analysis. The scale bars are 100 μm.

Principle of the HAUP method

The principle of the HAUP method is to measure the intensities of emergent light passing through a polarizer, crystal sample, and then analyzer as azimuth angles of the polarizer and analyzer are independently altered. We briefly explain the basic formula of the HAUP method. Details of the principle of the original[1–3] and the extended HAUP methods have been described elsewhere.[4–6] The generalized HAUP (G-HAUP) apparatus shown in Figure S2 employs a simple optical system that contains only two optical elements: a polarizer (*P*) and an analyser (*A*). The vibrational direction of the transmitted light through the *P* is orthogonal to that passing through the *A* (*i.e.*, the crossed Nicols position).

Due to this simple optical configuration, systematic errors, except those relating to the *P* and *A*, are excluded.[3] In the HAUP method, systematic errors originating from parasitic ellipticities of *P* and *A* (*p* and *q*, respectively) and a small error angle (δY, attributed to the displacement of the crossed Nicols configuration) are evaluated and eliminated. Here, we define θ as an azimuth angle of *P* from an arbitrary origin; *Y* as the azimuth angle of *A* from the crossed Nicols position of the arbitrary origin of *P*; θ_0 as an extinction position angle (*i.e.*, $\left(\frac{\partial(I/I_0)}{\partial\theta}\right)_{\Upsilon'=0} = 0$) of *P* from the arbitrary origin; θ' as the azimuth angle of *P* from θ_0; and Y' as the azimuth angle of *A* from δY. That is, $\theta = \theta_0 + \theta'$ and $Y = \delta Y + Y'$. The values of θ' and Y' can be measured accurately in the practical HAUP experiment. The clockwise direction from the viewpoint of an observer is defined as the positive direction for all angles.

The ratio, Γ, of the intensity of transmitted light and intensity of incident light, *I* and I_0, respectively, are represented as follows:

$$\Gamma(\theta', Y') = I/I_0 = A''(\theta') + B''(\theta')Y' + C''Y'^2, \tag{S1}$$

$$A''(\theta') = H''_{11} + H''_{12}\theta' + H''_{13}\theta'^2, \tag{S2}$$

$$B''(\theta') = H''_{21} + H''_{22}\theta', \tag{S3}$$

$$C'' = H''_{31}. \tag{S4}$$

where,

$H''_{11} \rightarrow$ independent of θ' and Υ'.

$$H''_{12} = 0,$$

$$H''_{13} = e^E + e^{-E} - 2\cos\Delta, \tag{S5}$$

$$H''_{21} = -b'_1 p + b'_2 q + a_1 \delta\Upsilon + 2c_1 k' - 2c_2(\sin\Delta)k, \tag{S6}$$

$$H''_{22} = 2(e^E - \cos\Delta), \tag{S7}$$

$$H''_{23} = e^E, \tag{S8}$$

where,

$$a_1 = \frac{2\sin^2\Delta}{e^E + e^{-E} - 2\cos\Delta},$$

$$b'_1 = -\frac{2(e^{-E} - \cos\Delta)\sin\Delta}{e^E + e^{-E} - 2\cos\Delta},$$

$$b'_2 = -\frac{2(e^E - \cos\Delta)\sin\Delta}{e^E + e^{-E} - 2\cos\Delta},$$

$$c_1 = \frac{K}{K^2+1} = \frac{E/\Delta}{(E/\Delta)^2+1},$$

$$c_2 = \frac{1}{K^2+1} = \frac{1}{(E/\Delta)^2+1}.$$

The extinction position angle, θ_0, can be expressed under the same approximation as follows:

$$\theta_0 = -a_2(p+q) - b_2\delta\Upsilon + c_1 k + c_2 k' + N, \tag{S9}$$

where

$$a_2 = \frac{\sin\Delta}{e^E + e^{-E} - 2\cos\Delta},$$

$b_2 = \frac{e^E - \cos\Delta}{e^E + e^{-E} - 2\cos\Delta}$.

Here, N is the difference of θ_0 from its absolute value. Here, Δ and E represent the phase difference and the total linear dichroism of the sample, respectively. k and k' represent the ellipticity derived from circular birefringence (CB) and circular dichroism (CD) of the sample, respectively. Using these quantities, linear birefringence (LB), linear dichroism (LD), circular birefringence (CB), and circular dichroism (CD) are expressed as follows:

$$\mathrm{LB} = n_s - n_f \equiv \frac{\Delta\lambda}{2\pi d}, \tag{S10}$$

$$\mathrm{LD} = m_s - m_f \equiv \frac{E\lambda}{2\pi d}, \tag{S11}$$

$$\mathrm{CB} = n_L - n_R \equiv \frac{\Delta k\lambda}{\pi d} = 2\mathrm{k}\,\mathrm{LB}, \tag{S12}$$

$$\mathrm{CD} = m_L - m_R \equiv -\frac{\Delta k'\lambda}{\pi d}. \tag{S13}$$

where subscripts s and f are axes of the slow and fast light rays, subscripts R and L are the right and left circular polarization, n is the refractive index, m is the absorption coefficient, λ is the wavelength of incident light, and d is the thickness of the sample, respectively.

In the HAUP method, the values of LB, LD, CB and CD are determined by the following procedure:

(i) The intensities of light, I, were measured as double functions of θ' and Υ'. The values of $I_0 \cdot H''_{ij}$ (i, j = 1, 2, 3) at each θ' position and θ_0 are determined by least-squares fittings using eqs S1–S4. The values of Δ, E and I_0 were calculated from the θ' dependences of H''_{13}, H''_{22} and H''_{31}, *i.e.*, eqs S5, S7 and S8. It should be noted that this procedure provides only the recorded phase difference, Δ_r ($0 \le \Delta_r \le \pi$). The real value of Δ was obtained using the relationship $\Delta = 2n\pi \pm \Delta_r$, where n is usually measured by using a Berek compensator. As an example, raw experimental results from the analysis of enol-(*S*)-**1** without UV irradiation at 293K are shown in Figure S3. The thickness of the sample was 6.5 μm which was measured by laser microscopy. From eqs S10 and S11, LB and LD were obtained by normalizing with the sample thickness, as shown in Figure S6a.

(ii) For extracting CB and CD from experimental data, reasonable procedures for removing the systematic errors are essential for the HAUP method. Since the value of p is independent of the sample setting, it has been already determined by a preceding experiment with an achiral crystal $LiNbO_3$ or MgF_2. Using this procedure, HAUP measurements of various crystals have been successfully performed.[4, 6, 7–9] For this study, the p value at 293K was determined to be 1.0×10^{-4} by the wavelength dependence measurements at 293 K of achiral MgF_2 crystal that was cut in the plane perpendicular to the a-axis.

We make successive approximations for determining the values of q and $\delta\Upsilon$. From eq S12, optical rotatory power (ORP) is defined as follows:

$$\mathrm{ORP} = \frac{\pi}{\lambda}\mathrm{CB} = \frac{\pi}{\lambda}2\mathrm{k}\,\mathrm{LB} = \frac{\Delta k}{d}. \tag{S14}$$

Additionaly, the ORP dispersion (ORD) spectra is related to the absorption spectrum of the optical active sample by the Drude expression[10] as follows:

$$\mathrm{ORP} = \sum_j \frac{A_j}{\lambda^2 - \lambda_j^2}, \tag{S15}$$

where λ_j is the wavelength of transition from the ground state to the excited state j, and A_j is a constant depending on the absorption strength of this transition. Therefore, we assumed that k is dependent on λ from eqs S14 and S15 as follows:

$$k = \frac{d}{\Delta}\sum_j \frac{A_j}{\lambda^2 - \lambda_j^2}, \tag{S16}$$

By assuming that k is dependent of λ (eq S16) and $k' = 0$ in the wavelength regions, where the sample has no absorption, the optimum values of q, $\delta\Upsilon$ and N are obtained by least-squares fittings using eqs S6 and S9 and the p value. In the case of the crystals enol-**1** both without and with UV irradiation, we made the

following approximations: (α) k is dependent of λ at the wavelength above 600 nm without UV irradiation as follows:

$$k = \frac{A'_{330}}{\Delta(\lambda^2 - 330^2)}, \quad \text{(S17)}$$

where $A'_{330}=A_{330}\times d$. With UV irradiation, k is represented as follows:

$$k = \frac{A'_{330}}{\Delta(\lambda^2 - 330^2)} + \frac{A'_{460}}{\Delta(\lambda^2 - 460^2)}, \quad \text{(S18)}$$

where $A'_{460}=A_{460}\times d$. (β) k' is nearly zero at the wavelength above 550 nm because the solution CD spectra shows no absorbance in this wavelength region.

The systematic error parameters q and δϒ determined by least-squares fittings are as follows:

$q = -2.36 \times 10^{-4}$

$\delta\Upsilon = 1.38 \times 10^{-4}$.

The values of q and δϒ obtained by least-squares fittings for any other experimental data in this study varied between 10^{-4}–10^{-3} and 10^{-5}–10^{-3}, respectively. In comparison with previous studies[9,11,12], these values are acceptable.

The values of k and k' are calculated by introducing the obtained systematic errors, Δ and E to eqs S6 and S9, as shown in Figure S4. Finally CB and CD are determined from eqs S12 and S13, as shown in Figure S6c.

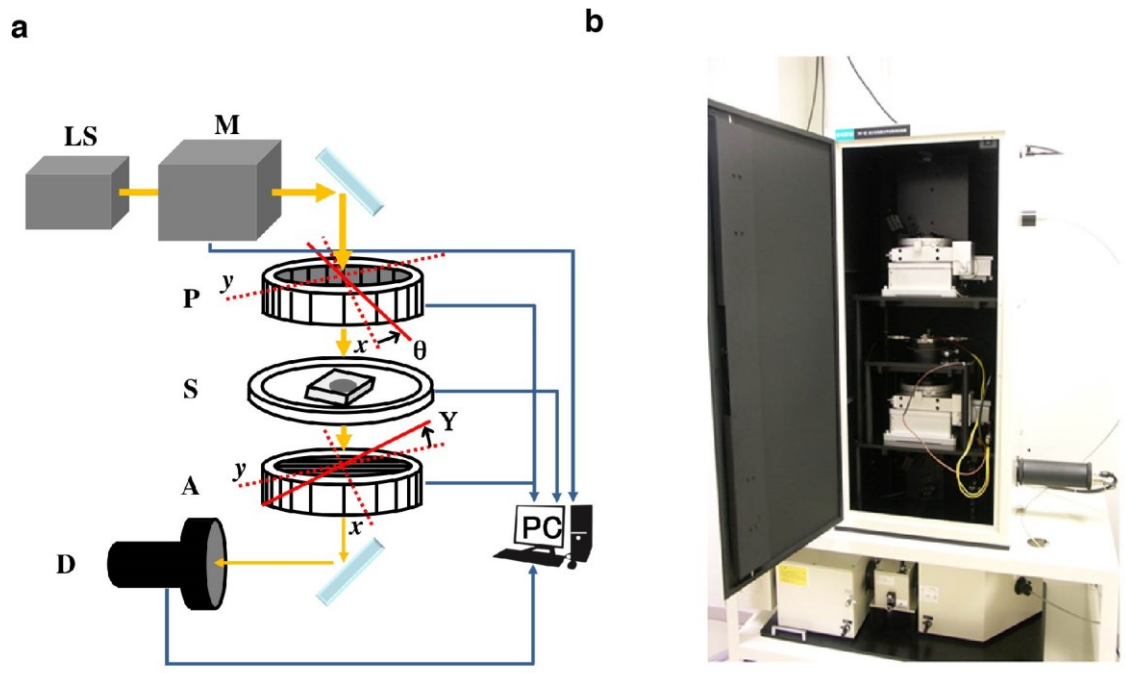

Figure S2. (a) Schematic drawing and (b) photograph of the G-HAUP apparatus. LS: light source; M: monochromator; P: polarizer; S: sample stage with temperature control unit; A: analyser; D: detector. Here, θ represent the azimuthal angle from an arbitrary origin and ϒ represent the deflecting angle of A from the crossed Nicols position.

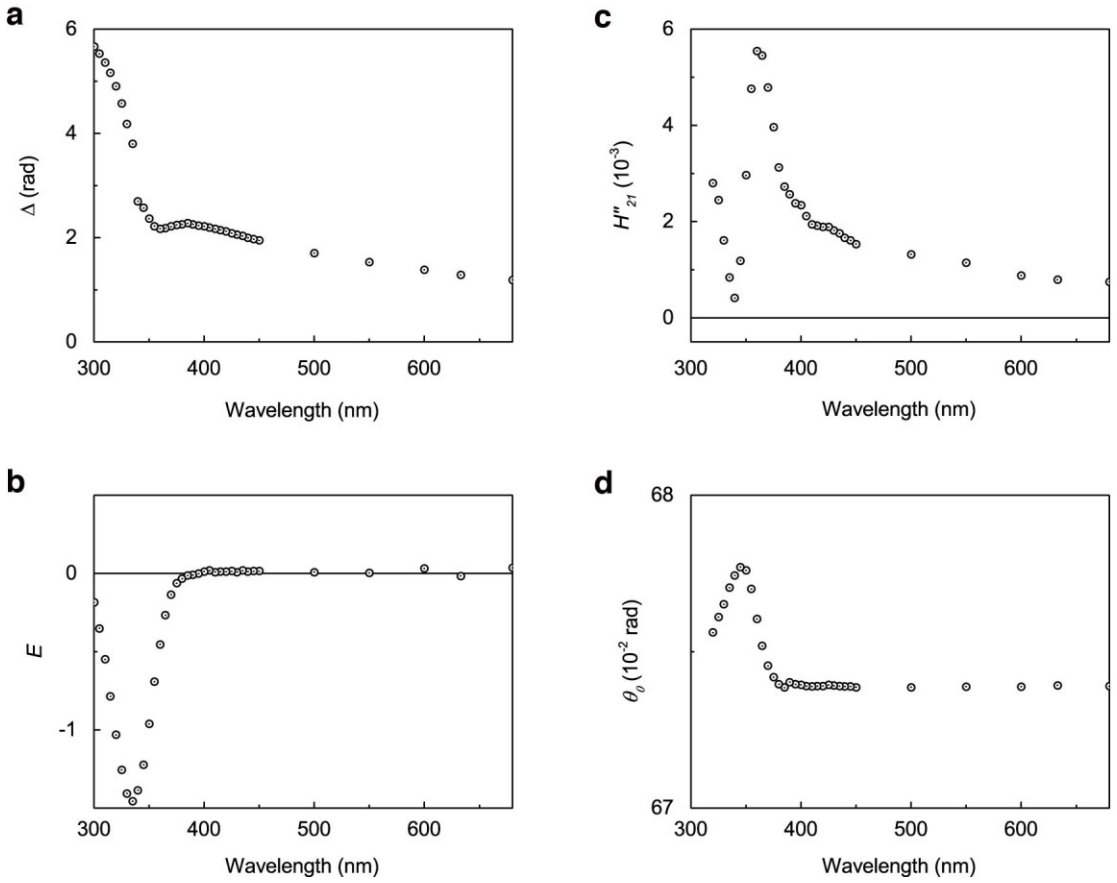

Figure S3. Raw experimental results from the analysis of enol-(*S*)-**1** on the (001) face at 293K: (a) the phase difference (real value), (b) the total linear dichroism, (c) H''_{21} and (d) the extinction position angle.

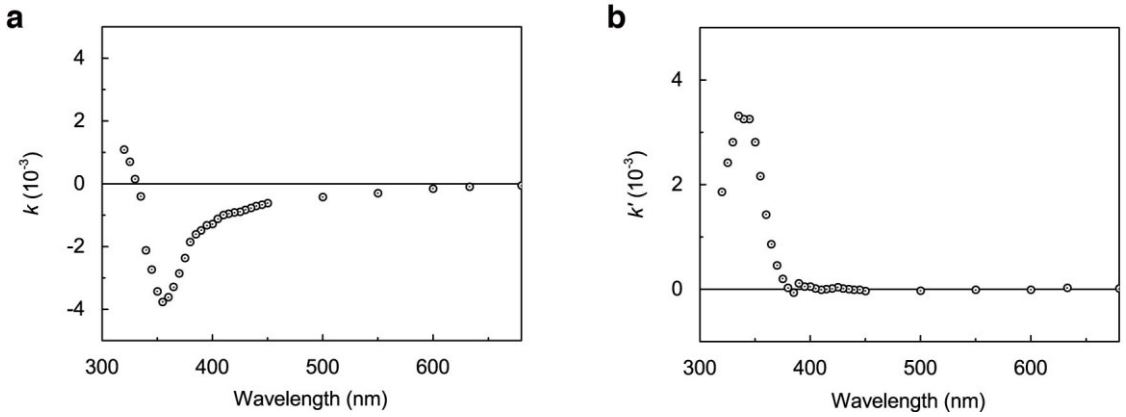

Figure S4. (a) *k* and (b) *k'* spectra calculated from Figure S3.

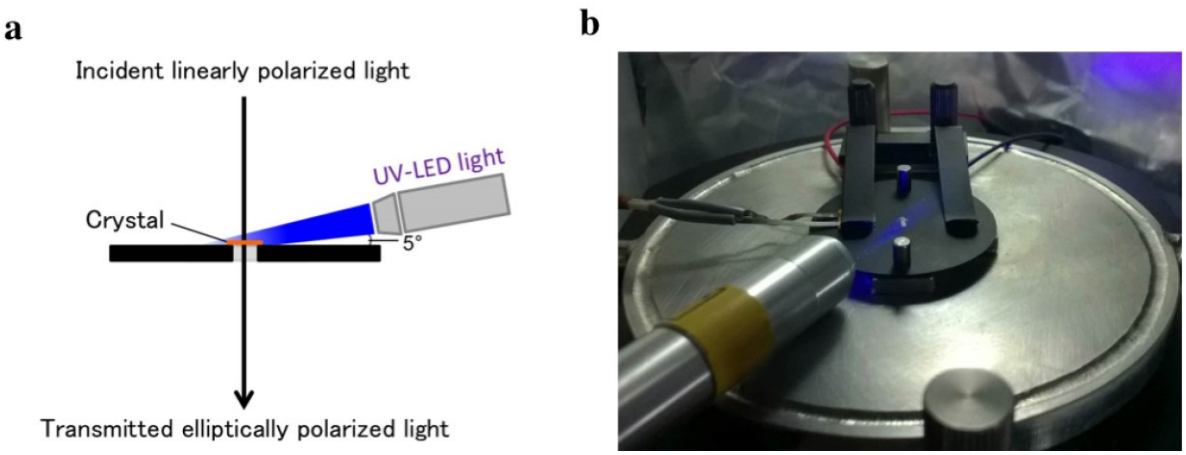

Figure S5. (a) Schematic representation and (b) photograph of UV light irradiation for the HAUP measurement.

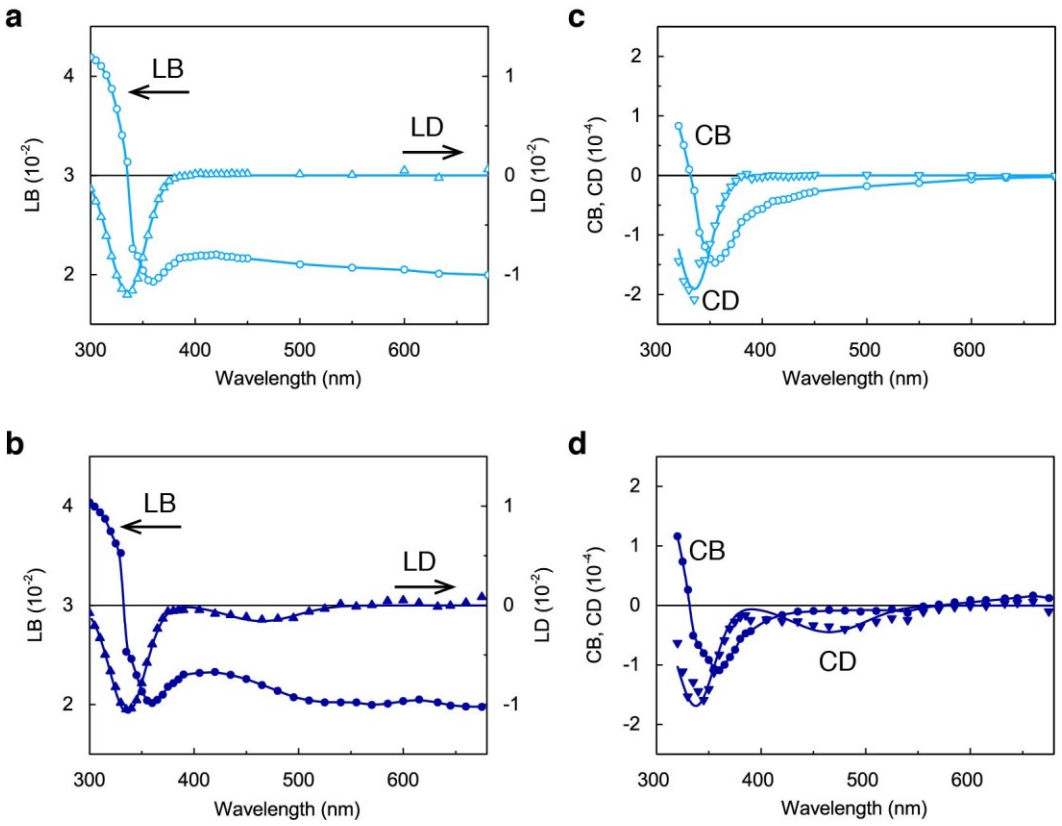

Figure S6. Optical anisotropic and chiroptical spectra of enol-(*S*)-**1** crystal on the (001) face: LB (left vertical axis, light blue circle) and LD (right vertical axis, light blue triangle) (a) without and (b) with UV irradiation: CB (dark blue circle) and CD (dark blue triangle) (c) without and (d) with UV irradiation. The curve lines of LB and CB are served as an eye guide, and those of LD and CD are fitted by Gaussian functions. All the graphs indicate that the Kramers–Kronig relationship hold between (a, b) the LD and LB as well as (c, d) the CD and CB before and under continuous UV irradiation.

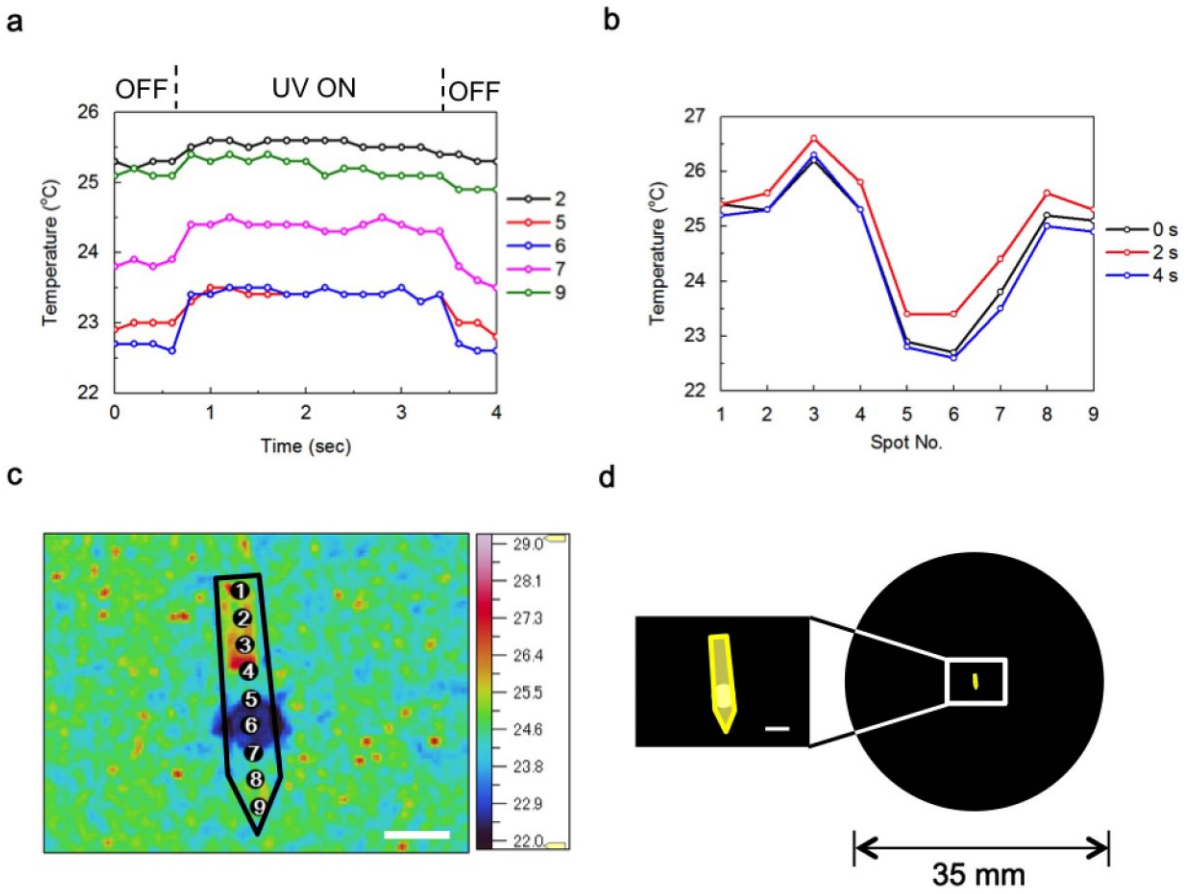

Figure S7. (a) Time dependence and (b) spot dependence of surface temperature change of the enol-(*S*)-**1** crystal upon UV (365 nm) irradiation measured by IR thermometer (Apiste FSV-2000). (c) IR thermographic image. The crystal form is lined in black color. The spot numbers are manually defined. (d) The right drawing represents the thin platelike crystal fixed on a Cu sample plate with a pinhole of 0.5 mm in diameter. The left drawing represents the enlarged view of the white rectangle box area. The white scale bar is 0.5 mm.

The surface temperature at the spots 5–7 inside the pinhole immediately elevated by 0.6–0.9 degree upon UV irradiation with the UV-LED light at 365 nm, and returned to the initial temperature after stopping irradiation. The reason that the temperature at the place (spots 1–4, 8, and 9) except the pinhole was higher than that inside the pinhole (spots 5–7) is likely due to the better heat absorption by the black Cu sample plate.

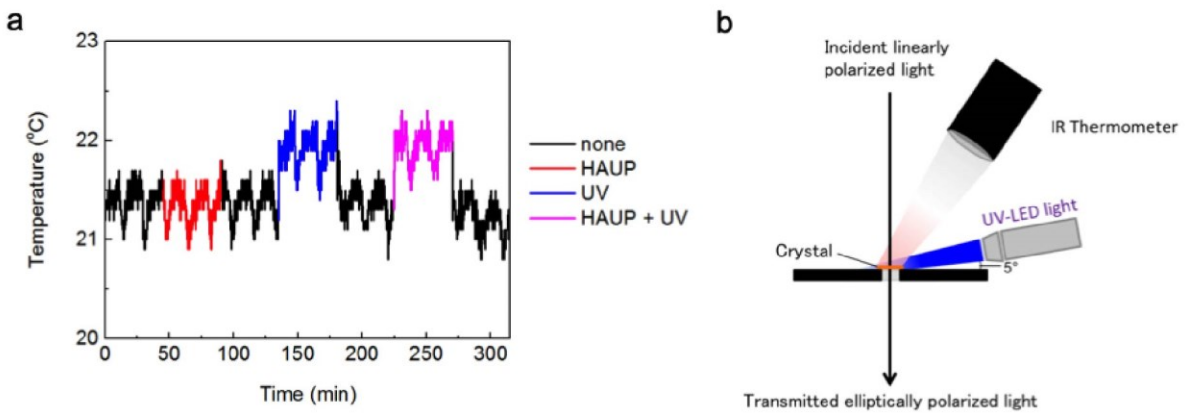

Figure S8. (a) In situ surface temperature profile of the enol-(*S*)-**1** crystal measured by IR thermometer (JAPAN SENSOR TMHX-CSE0500-0040H0.7) and (b) schematic representation of *in situ* surface temperature measurement. In the graph (a), the thin platelike crystal fixed on the Cu plate was mounted on the sample stage of the HAUP apparatus. The measurement area of the IR thermometer was 0.7 mm in diameter. Black line: none means no incident light of the HAUP (blank). Red line: HAUP means that the sample was irradiated by the incident light (330 nm) during the HAUP measurement. Blue line: UV means that the sample was irradiated with UV-LED light at 365 nm for proceeding the photoisomerization to the *trans*-keto-(*S*)-**1**. Pink line: HAUP + UV means that the sample was irradiated by both the incident light of HAUP (330 nm) and UV-LED light (365 nm). The each measurement time interval was 45 min.

The temperature profile shows that the surface temperature of the crystal sample did not change by the incident light (330 nm) of the HAUP. In contrast, the surface temperature elevated by around 0.5 degree by the irradiation with the UV-LED light at 365 nm. Periodical temperature drop of 18 min interval was due to the ON/OFF of room air-conditioner. It is most probably thought that the slight heating of crystals caused the decrease of thickness due to the quite long time for about 3 days required for the HAUP measurement.

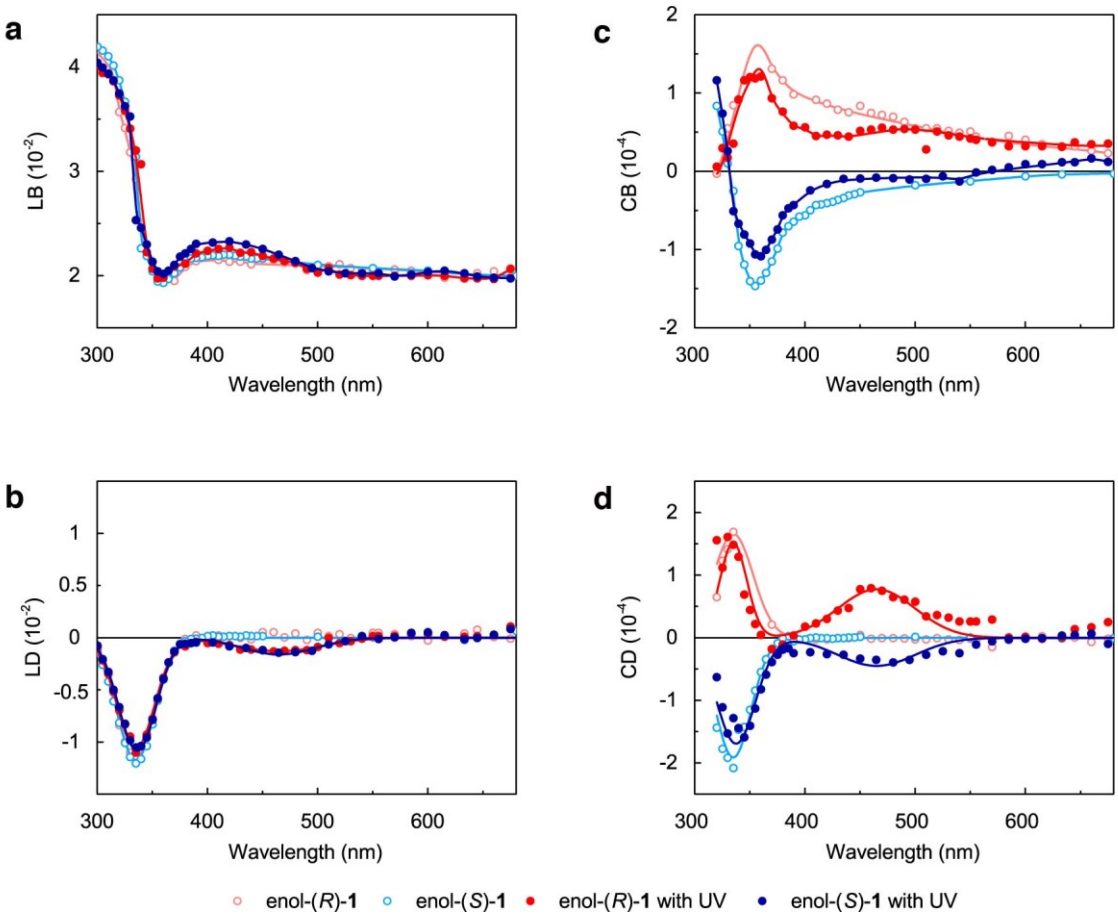

Figure S9. Optical anisotropic and chiroptical spectra of enol-(*S*)-**1** and enol-(*R*)-**1** crystals on the (001) face: (a) LB, (b) LD, (c) CB, and (d) CD. These properties were measured with the G-HAUP without and under continuous UV light irradiation at 365 nm. The curve lines are served as an eye guide (a, c) and are fitted by Gaussian functions (b, d).

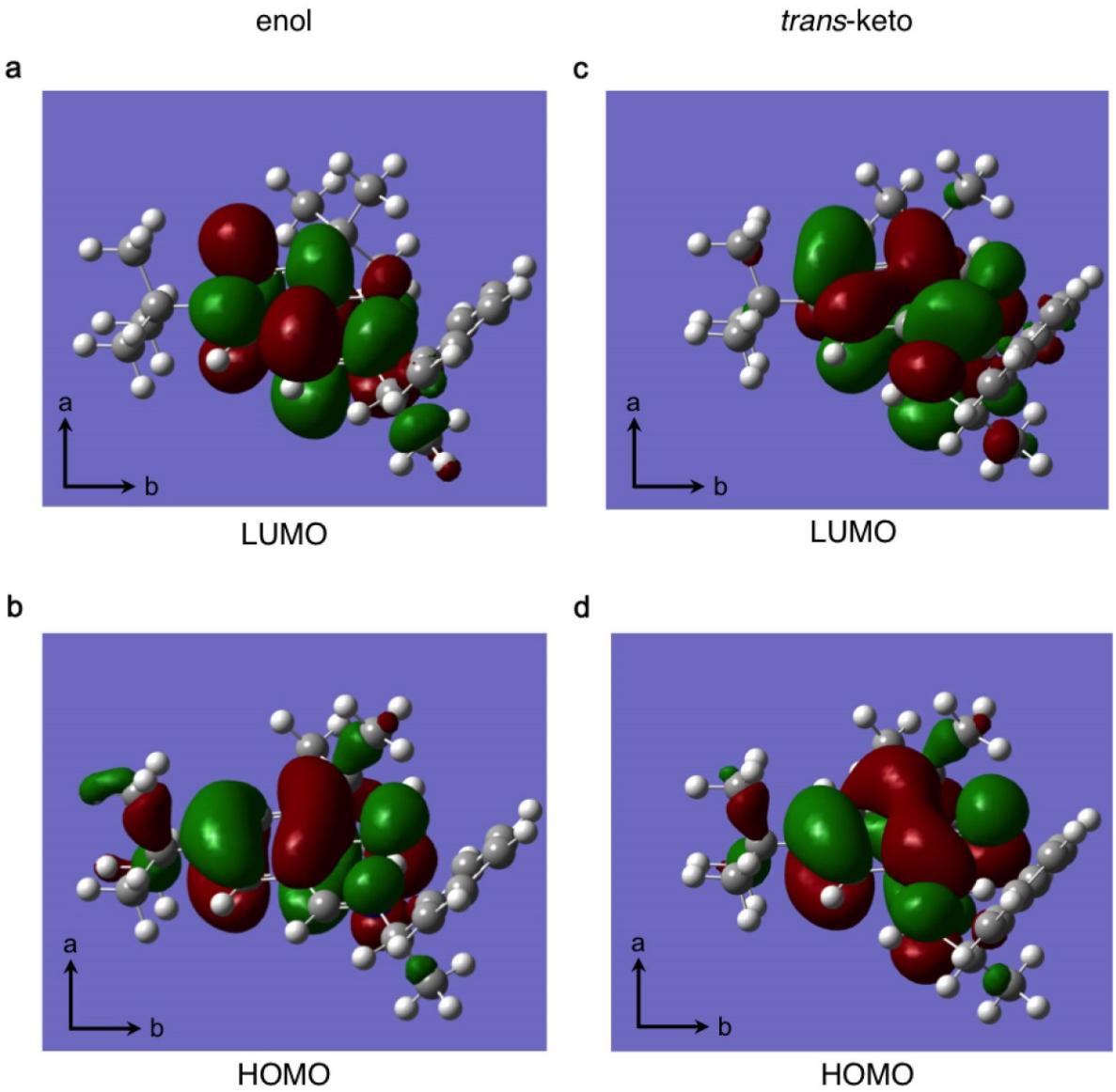

Figure S10. Visualization of (b, d) HOMO and (a, c) LUMO orbitals involved in the electronic transitions of calculated (a, b) enol-(*S*)-**1** and (c, d) *trans*-keto-(*S*)-**1**. All molecules are projected on the (001) face. Orbitals of HOMO and LUMO are of π type. See the Experimental Section in the main text for calculation details.

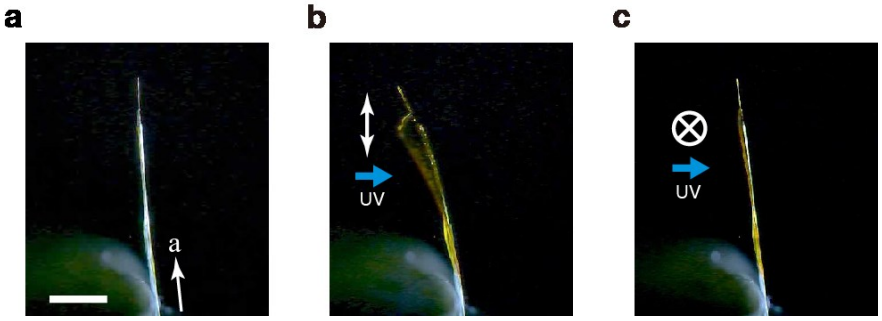

Figure S11. Bending behavior of a platelike enol-(*S*)-**1** crystal (4516 μm long × 380 μm wide × 97 μm thick) (a) before and upon irradiation from left to the (00–1) face with (b) linearly polarized UV light parallel and (c) perpendicular vibration direction to the *a* axis. The scale bar is 1 mm. To produce a linearly polarized light, Glan-Tompson prism polarizer was applied between the sample and the UV LED light illuminator. Because of the presence of the Glan-Tompson prism polarizer, the intensity of the UV light was decreased (30 mW cm^{-2}).

Figure S11a shows the frontal (0–10) face with the longitudinal direction along the *a* axis, whose lower portion was fixed to the needle with an adhesive and the upper portion was free. Upon irradiation from left with linearly polarized UV light at 365 nm almost parallel to the *a* axis, the crystal bent (Figure S11b and Movie S3). According to the relationship between the direction of twisting and the face of enol-(*S*)-**1** crystal irradiated with UV light (Figure 3), the irradiated face was determined to be the (00–1) face. On the other hand, polarized UV light almost perpendicular to the *a* axis did not induce any bending motion (Figure S11c and Movie S4). We shortly explored the possible mechanism of this bending with twisting motion of thin platelike enol-(*S*)-**1** crystal depending on the vibration direction of linearly polarized light. Upon linearly polarized UV irradiation of the (00–1) face almost parallel to the *a* axis, both the length and width along the *a* and *b* axes shrink to the diagonal direction near the irradiated surface due to the photoisomerization to the *trans*-keto-(*S*)-**1** molecules. In contrast, both the length and the width do not change at the back surface due to lack of penetration of the irradiated light and no occurrence of photoisomerization. Hence the wide platelike crystal bends toward the light source with twisting motion in right-handed helix (Figure S11b). Upon linearly polarized UV irradiation of the (00–1) face almost perpendicular to the *a* axis, both the length and width along the *a* and *b* axes change a very little near the irradiated surface due to the low photoisomerization to the *trans*-keto-(*S*)-**1** molecules. Similarly, both the length and the width do not change at the back surface due to lack penetration of the irradiated light. Hence the wide platelike crystal scarecely bend toward the light source (Figure S11c).

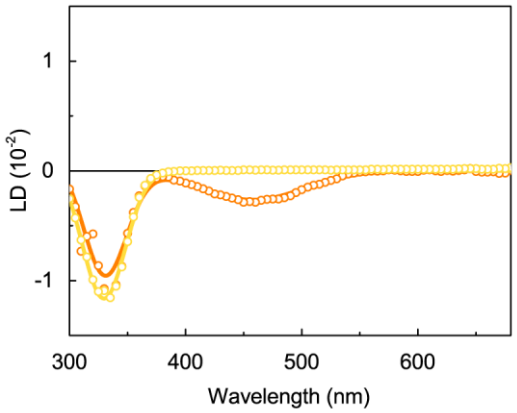

Figure S12. LD spectra of the enol-(*S*)-**1** crystal before (yellow open circle) and under continuous UV light irradiation (orange open circle) calculated from the linearly polarized absorption spectra in Figure 5 of the main text. The curve lines are fitted by Gaussian functions.

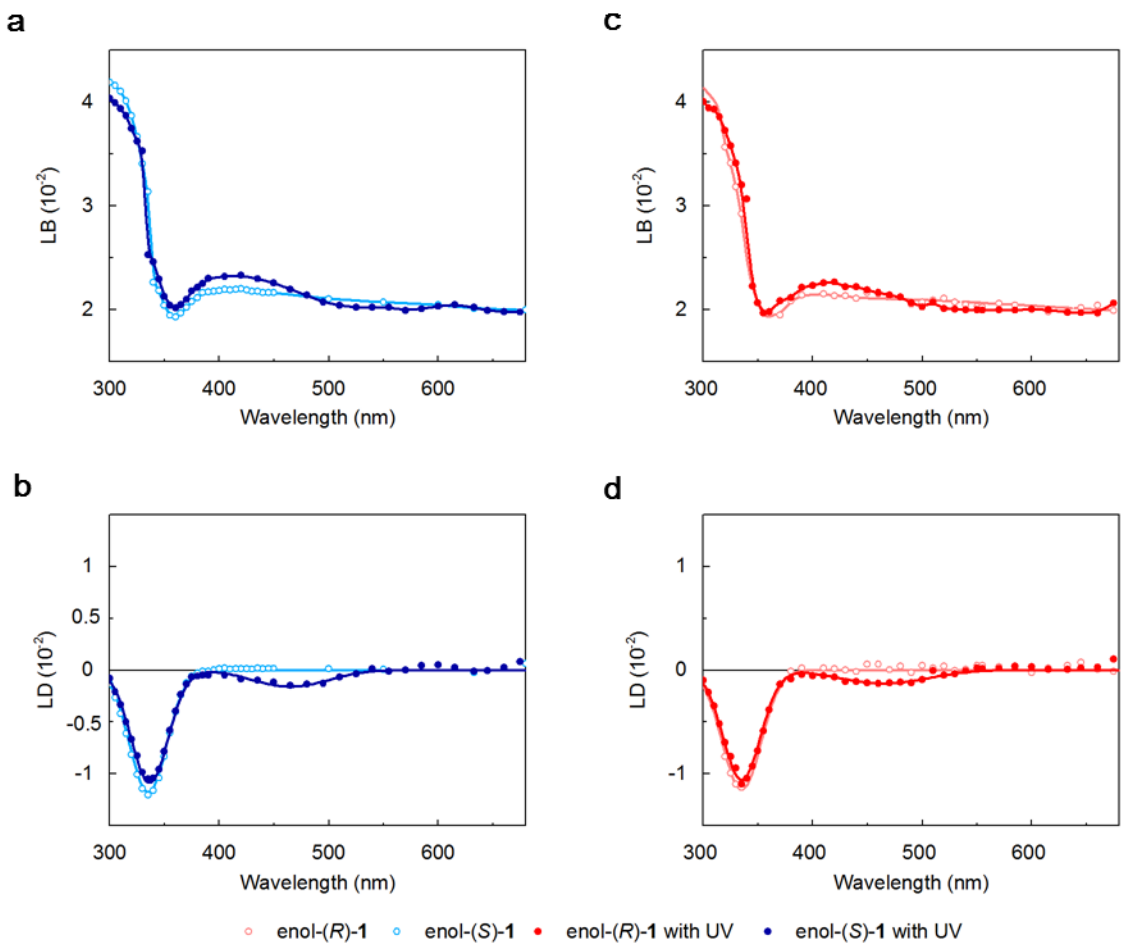

Figure S13. Optical anisotropic properties of (a, b) enol-(*S*)-**1** and (c, d) enol-(*R*)-**1** crystals on the (001) face: (a, c) LB and (b, d) LD without and with UV irradiation. The curve lines are served as an eye guide (a, c) and are fitted by Gaussian functions (b, d).

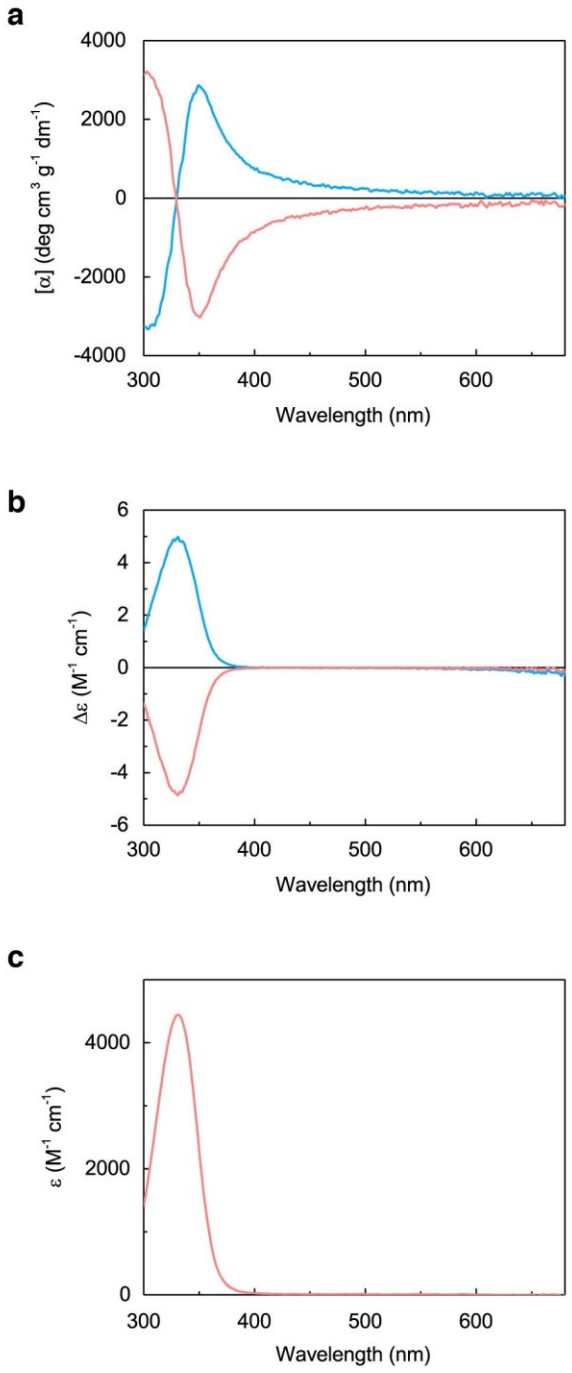

Figure S14. (a) Optical rotation, (b) CD, and (c) UV-Vis absorption spectra of enol-(*S*)-**1** (blue) and enol-(*R*)-**1** (pink) in hexane (c 0.016). Concentration in g (100 mL)$^{-1}$.

In hexane, optical rotation spectra of enol-(*S*)-**1** and enol-(*R*)-**1** exhibited anomalous dispersions of positive and negative peaks at 351 nm with change in signs at the positive and negative CD peaks at 331 nm, respectively. Strong absorption peak at 328 nm was observed. We have obtained almost same results in acetonitrile (not shown here). Optical rotation spectra of enol-(*S*)-**1** and enol-(*R*)-**1** exhibited anomalous dispersions of positive and negative peaks at 348 nm with change in signs at the positive and negative CD peaks at 326 nm, respectively. Strong absorption peak at 327 nm was observed.

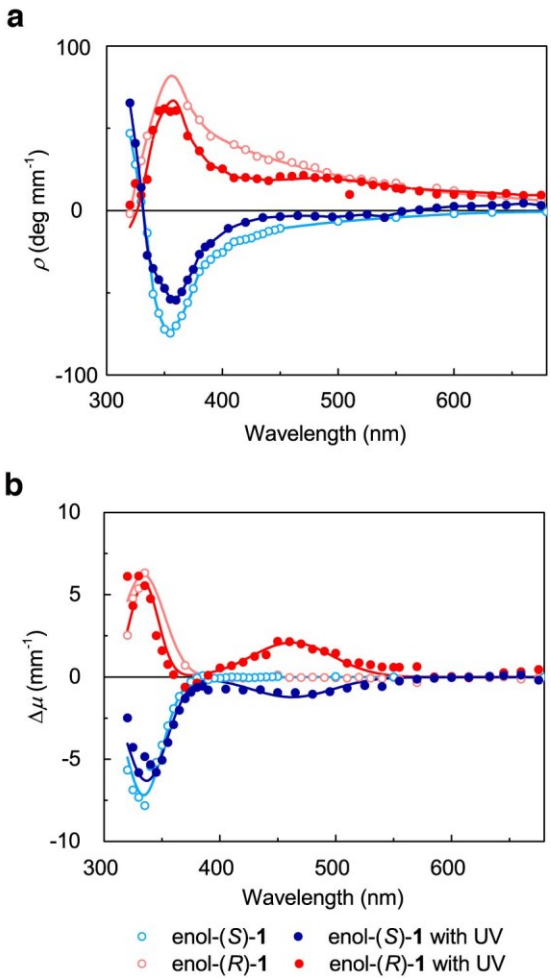

Figure S15. (a) ORP and (b) CD spectra of enol-(*S*)-**1** and enol-(*R*)-**1** crystals on the (001) face before and under continuous UV irradiation. The curve lines are served as an eye guide (a) and are fitted by Gaussian functions (b).

Table S1. Cartesian Atomic Positions for enol-(*S*)-1 generated from the calculated crystal structure.

Atom	x (Å)	y (Å)	z (Å)
C	3.003	6.139	13.488
C	2.184	6.963	12.67
C	1.445	6.386	11.607
C	1.559	5.008	11.439
H	0.987	4.542	10.639
C	2.362	4.166	12.233
C	3.084	4.759	13.252
H	3.722	4.172	13.91
C	3.77	6.704	14.569
H	4.41	6.021	15.151
C	3.77	9.348	16.873
C	4.043	9.274	18.24
H	4.78	8.557	18.598
C	3.385	10.104	19.147
H	3.616	10.028	20.21
C	2.439	11.02	18.688
H	1.929	11.685	19.386
C	2.145	11.089	17.326
H	1.404	11.801	16.965
C	2.805	10.254	16.427
H	2.566	10.296	15.366
C	4.57	8.509	15.9
H	5.046	7.68	16.458
C	5.671	9.355	15.248
H	5.215	10.148	14.639
H	6.304	8.737	14.598
H	6.293	9.818	16.022
C	0.581	7.244	10.681
C	1.471	8.275	9.961
H	0.851	8.9	9.301
H	2.227	7.767	9.346
H	1.982	8.927	10.677
C	-0.517	7.963	11.485
H	-1.176	7.232	11.973
H	-1.133	8.571	10.805
H	-0.095	8.621	12.252
C	-0.117	6.403	9.607

H	-0.798	5.66	10.048
H	0.606	5.882	8.961
H	-0.717	7.068	8.971
C	2.383	2.667	11.967
C	0.976	2.093	12.205
H	0.964	1.01	12.018
H	0.238	2.57	11.543
H	0.663	2.265	13.246
C	2.807	2.404	10.514
H	2.126	2.89	9.802
H	2.799	1.324	10.308
H	3.82	2.79	10.332
C	3.365	1.94	12.888
H	4.392	2.305	12.744
H	3.347	0.865	12.67
H	3.094	2.083	13.942
N	3.723	7.973	14.846
O	2.133	8.288	12.917
H	2.762	8.45	13.741

Table S2. Cartesian Atomic Positions for *trans*-keto-(*S*)-1 generated from the calculated crystal structure.

Atom	x (Å)	y (Å)	z (Å)
C	2.939	6.56	13.612
C	2.103	7.271	12.62
C	1.378	6.437	11.663
C	1.513	5.077	11.764
H	0.972	4.453	11.055
C	2.327	4.386	12.722
C	3.034	5.138	13.62
H	3.67	4.653	14.364
C	3.63	7.398	14.475
H	3.48	8.462	14.288
C	4.258	8.832	17.265
C	4.425	8.636	18.639
H	5.193	7.948	18.998
C	3.629	9.32	19.562
H	3.795	9.169	20.629
C	2.651	10.211	19.117
H	2.038	10.759	19.833
C	2.475	10.411	17.746
H	1.723	11.119	17.394
C	3.272	9.726	16.832
H	3.129	9.908	15.77
C	5.165	8.124	16.269
H	5.917	7.562	16.841
C	5.878	9.115	15.35
H	5.16	9.687	14.749
H	6.564	8.604	14.661
H	6.444	9.83	15.957
C	0.568	7.093	10.552
C	1.545	7.864	9.646
H	0.995	8.312	8.81
H	2.299	7.18	9.232
H	2.053	8.661	10.203
C	-0.501	8.045	11.117
H	-1.202	7.498	11.76
H	-1.08	8.474	10.285
H	-0.05	8.86	11.691
C	-0.158	6.065	9.684

H	-0.87	5.469	10.273
H	0.538	5.383	9.175
H	-0.73	6.59	8.906
C	2.333	2.867	12.677
C	0.899	2.344	12.866
H	0.897	1.248	12.798
H	0.216	2.74	12.103
H	0.519	2.637	13.855
C	2.869	2.379	11.321
H	2.266	2.767	10.489
H	2.84	1.281	11.289
H	3.905	2.713	11.17
C	3.196	2.258	13.779
H	4.246	2.559	13.676
H	3.137	1.165	13.688
H	2.837	2.559	14.776
N	4.449	7.097	15.486
O	2.039	8.534	12.613
H	4.686	6.119	15.687

REFERENCES

(1) Kobayashi, J.; Uesu, Y. *J. Appl. Crystallogr.* **1983**, 16, 204–211.

(2) Kobayashi, J.; Kumomi, H.; Saito, K. *J. Appl. Crystallogr.* **1986**, 19, 377–381.

(3) Kobayashi, J.; Asahi, T.; Takahashi, S.; Glazer, A. M. *J. Appl. Crystallogr.* **1988**, 21, 479–484.

(4) Kobayashi, J.; Asahi, T.; Sakurai, M.; Takahashi, M.; Okubo, K.; Enomoto, Y. *Phys. Rev. B: Condens. Matter. Phys.* **1996**, 53, 11784–11790.

(5) Asahi, T.; Osaka, T.; Kobayashi, J. *Proc. SPIE* **2001**, 4467, 20–30.

(6) Tanaka, M.; Nakamura, N.; Koshima, H.; Asahi, T. *J. Phys. D: Appl. Phys.* **2012**, 45, 175303.

(7) Asahi, T.; Osaka, T.; Abrahams, S. C.; Miyazaki, R.; Asai, H.; Nanamatsu, S.; Kobayashi, J. *Proc. SPIE* **2003**, 5218, 223–232.

(8) Matsuki, R.; Asahi, T.; Kobayashi, J.; Asai, H. *Chirality* **2004**, 16, 286-293.

(9) Nakagawa, K.; Harper-Lovelady, H.; Tanaka, Y.; Tanaka, M.; Yamato, M.; Asahi, T. *Chem. Commun.* **2014**, 50, 15086–15089.

(10) Barron, L. D. *Molecular Light Scattering and Optical Activity*; Cambridge University Press: Cambridge, 2009.

(11) Asahi, T.; Nakamura, M.; Kobayashi, J.; Toda, F.; Miyamoto, H. *J. Am. Chem. Soc.* **1997**, 119, 3665–3669.

(12) Koshima, H.; Nagano, M.; Asahi, T. *J. Am. Chem. Soc.* **2005**, *127*, 2455–2463.